MONITORING THERMOSPHERIC DENSITY VARIATIONS WITH THE CHAMP SATELLITE

H. Lühr[1], M. Förster[1], C. Reigber[1], R. König[1],
A. A. Namgaladze[2,3], and R. Y. Yurik[3]

1 – GeoForschungsZentrum Potsdam, Telegrafenberg, D–14473 Potsdam, Germany
E-Mail : hluehr@gfz-potsdam.de
2 – Murmansk State Technical University, 13 Sportivnaya Street, 183010 Murmansk, Russia,
E–mail: Namgaladze@mstu.edu.ru
3 – Polar Geophysical Institute, Russian Academy of Sciences, 15 Halturina street,
183010 Murmansk, Russia, E–mail: Namgalad@polar.murmansk.su

ABSTRACT

A high resolution accelerometer for precise orbit determination will be part of the payload of the geoscience satellite CHAMP. On its low-Earth orbit ($< 450\ km$) the atmospheric drag will contribute a significant part to non gravitational forces. The average air drag will be two to three orders of magnitude higher than the resolution of the accelerometer. Density variations and winds caused by magnetic activity, enhanced UV irradiation or atmospheric waves will be detectable. To simulate numerically realistic parameters, we employed the Global Self–Consistent Model for the Thermosphere, Ionosphere and Protonosphere (GSM TIP). Both input and output quantities of the modelling will be measured in–situ along the spacecraft's orbital track. In a series of simulation runs the CHAMP satellite is flown through the temporally developing density anomalies at different heights. The obtained accelerations monitor very well the storm induced changes in density. This technique will be a powerful tool to test and improve atmospheric models.

Keywords: Accelerometer, Geomagnetic Storm, Thermosphere, Air Drag, Modelling.

1. INTRODUCTION

The geoscience satellite CHAMP with its prime scientific goals to determine the global distribution of gravity and magnetic fields is the first spacecraft which will carry a high resolution accelerometer for precise orbit determination at the satellite's center of gravity (CoG, cf. Figure 1). On its near–polar, low Earth orbit ($< 450\ km$), the atmospheric drag will contribute a significant part to non-gravitational forces acting on the satellite which results in a more or less rapid orbit decay. Due to the foreseen launch date (late 1999) the decay rate of CHAMP will depend sensitively on the phase and intensity of the forthcoming solar activity cycle (Figure 2). With a resolution of the accelerometer of $< 1 \times 10^{-8} m/s^2$ the average air drag will easily be resolvable.

In this paper we will show which kind of variabilities in density or winds caused by magnetic activity, enhanced UV irradiation or atmospheric waves will be detectable.

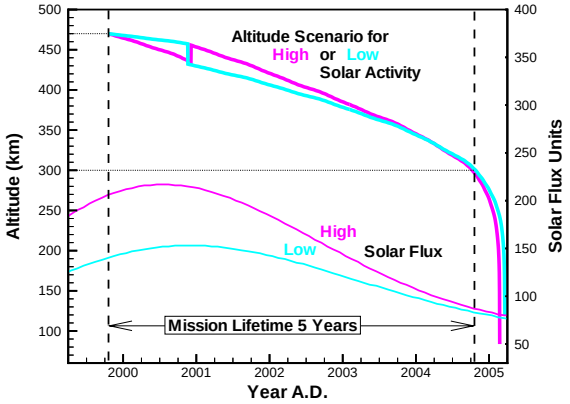

Figure 2: Orbital decay of the satellite CHAMP including orbit maintainance to insure a 5 years in–orbit life time.

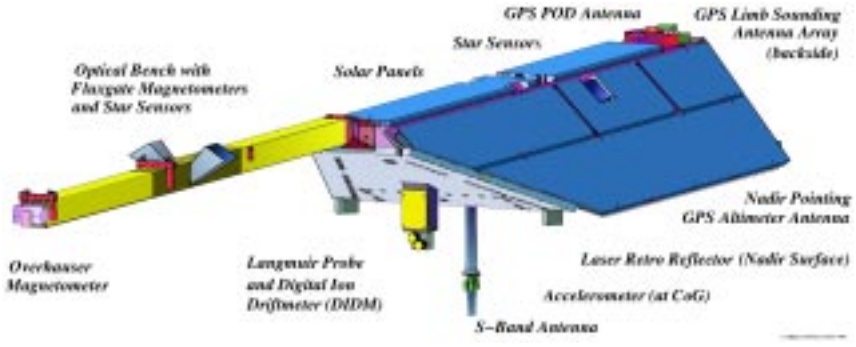

Figure 1: Schematic view of the CHAMP satellite.

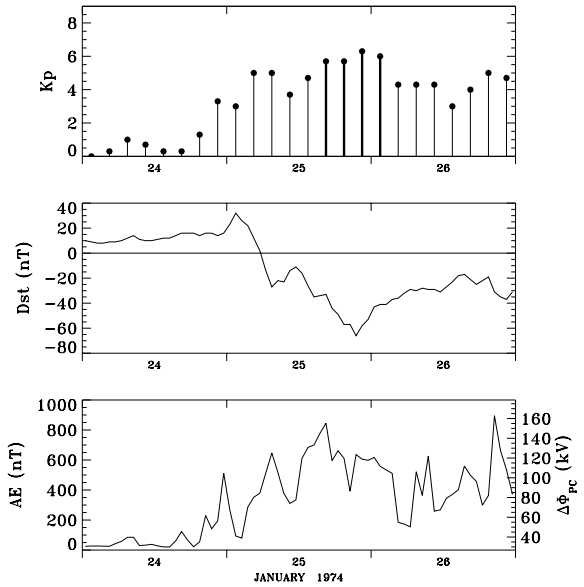

Figure 3: Activity indices Kp and Dst as well as the model input parameter $\Delta\Phi_{PC}$ plotted versus UT for the storm interval.

Our investigations are based on a global numerical modelling of the coupled system thermosphere, ionosphere, plasmasphere and magnetosphere applied to a rather typical, medium–active geomagnetic storm. During the CHAMP mission, with its elevated solar activity the occurence probability of such environmental disturbances will be high.

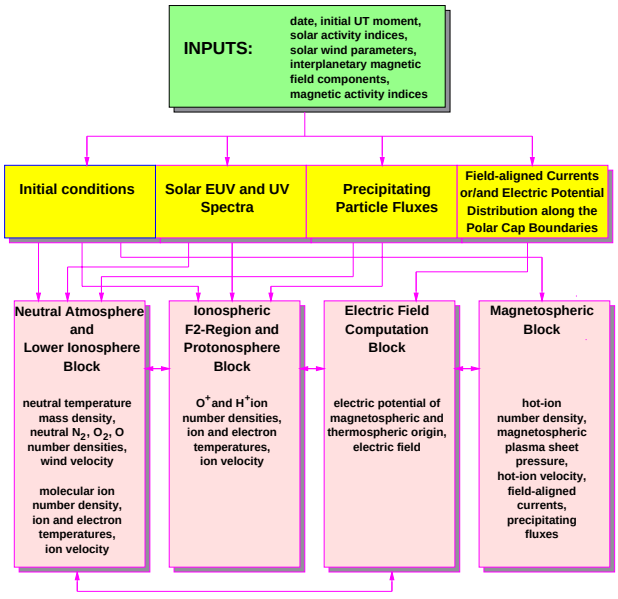

Figure 4: Structure of the Global Self-Consistent Model for the Thermosphere, Ionosphere and Protonosphere (GSM–TIP) with inputs, its main computational blocks and their outputs.

2. MAGNETIC STORM MODELLING

As an example we take the well-documented magnetic storm of Jan 25, 1974, (Wei & Förster, 1989; Förster *et al.*, 1992) to model the expected effects. Some geomagnetic activity indices for this time interval are given in Figure 3. The cross-polar potential ($\Delta\Phi_{PC}$) is estimated from the 3-hourly AE index according to (Weimer *et al.*, 1990) and serves as main model input parameter. The storm commenced at the beginning of Jan 25 and reached its main phase by the end of that day.

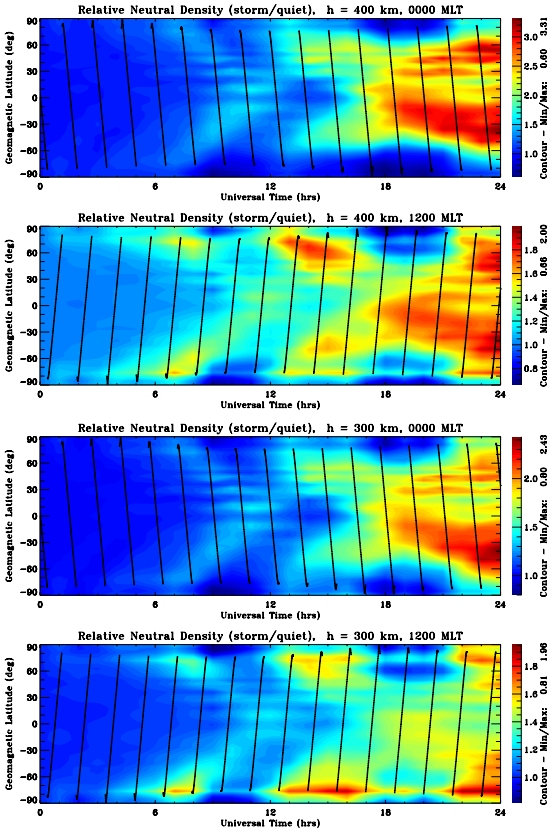

Figure 5: Neutral density ratio for the storm day Jan 25, 1974, with respect to the quiet time reference day prior to the storm. Shown are the time sectors 0000 MLT and 1200 MLT both for 400 km (a) and 300 km altitude (b). Satellite tracks are indicated by dotted lines.

Our tool for modeling the environmental conditions is the Global Self-Consistent Model for the Thermosphere, Ionosphere and Protonosphere (GSM TIP) (Namgaladze *et al.*, 1988; Namgaladze *et al.*, 1991). The model describes the thermosphere, ionosphere, and protonosphere of the Earth as a single system by means of numerical integration of the corresponding time-dependent three-dimensional continuity, momentum, and heat balance equations for neutral, ion, and electron gases as well as the equation for the electric field potential (see the schematic

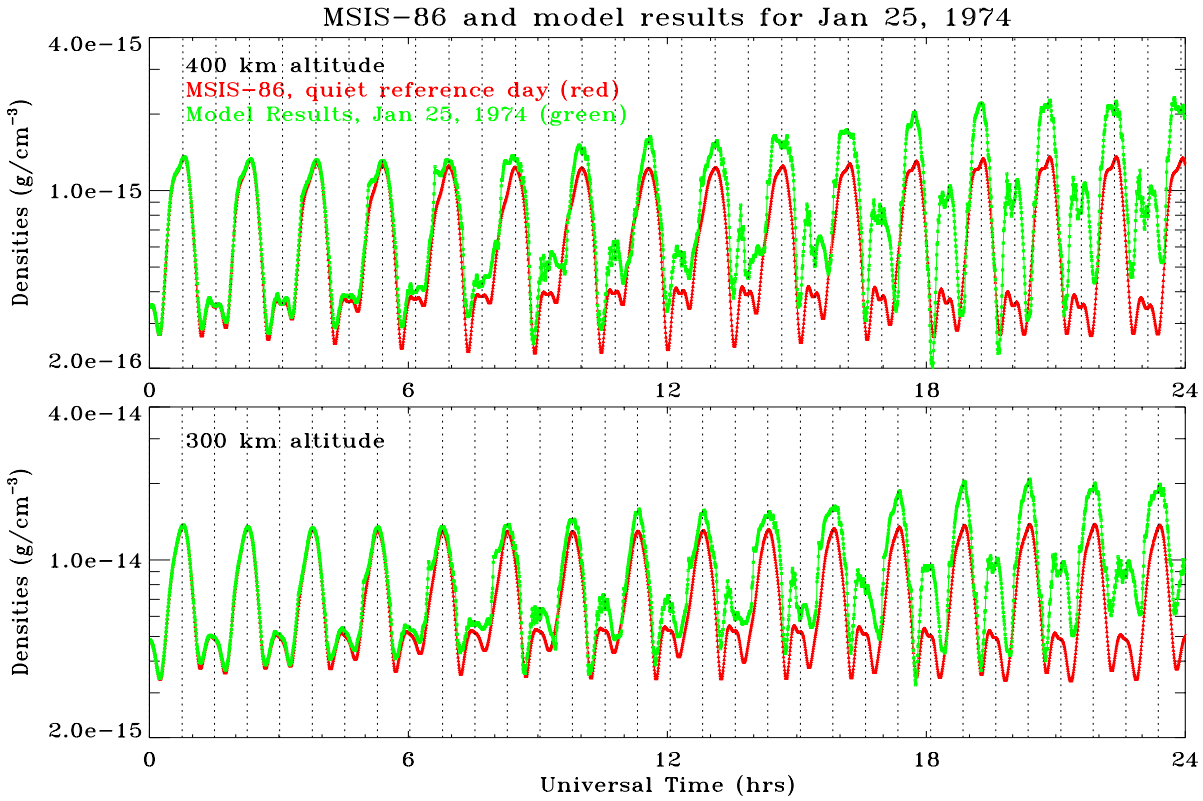

Figure 6: MSIS–86 and GSM TIP model densities along the satellite track for the orbits at 400 km (a) and 300 km altitude (b). Crossings of the geographic equator are indicated by vertical lines. At higher activities toward the end of the day the Model shows much more structures.

in Figure 4).

Required input parameters for the model are either the Region 1 FAC distribution or the cross-polar cap potential. In cases where these parameters have not been measured estimates have to be used derived from magnetic activity indices.

3. THERMOSPHERIC DENSITY

In a series of simulation runs we have flown the CHAMP satellite on a noon/midnight orbit through the temporally developing density anomalies during the modeled strom of Jan 25, 1974, at two characteristic heights (400 km and 300 km). Realistic numbers for the satellite shape and its cross section to mass ratio have been used. The temporal evolution of the global density disturbances are given for two MLT sectors as color plots over geomagn. latitude versus UT in Fig. 5.

The satellite is exposed to thermospheric density variations along the satellite track as shown in Fig. 6 for two different orbital heights and in comparison with the generally used MSIS–86 (or CIRA–86) empirical thermospheric model (Hedin, 1987). The overall trend is certainly similiar, but the GSM TIP model results show the more immediate reaction of the thermosphere on the magnetic storm forcings and, as in our example, the density differences can be as large as 100%. A blow–up of this plot in Fig. 7 shows the rich variety of realistic model density variations resulting, e.g., from local disturbances and travelling atmospheric waves. A similar, well measurable effect will result from air drag caused by thermospheric wind fields.

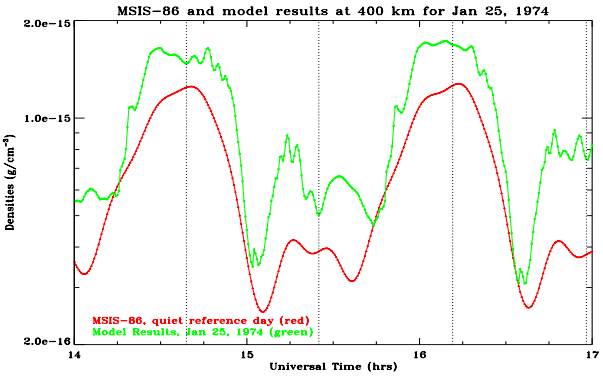

Figure 7: Details in neutral density like gravity waves are resolved by the GSM TIP model (cf. Fig. 5).

4. ORBITAL DRAG

The resulting orbital drag, finally, is shown in Figure 8 and a zoomed–in detail in Figure 9.

Shown are the acceleration estimates due to neutral air drag derived from the MSIS–86 model (blue) and from the GSM TIP model (purple) at 300 km and 400 km altitude. In all phases the drag is well above the resolution of the accelerometer.

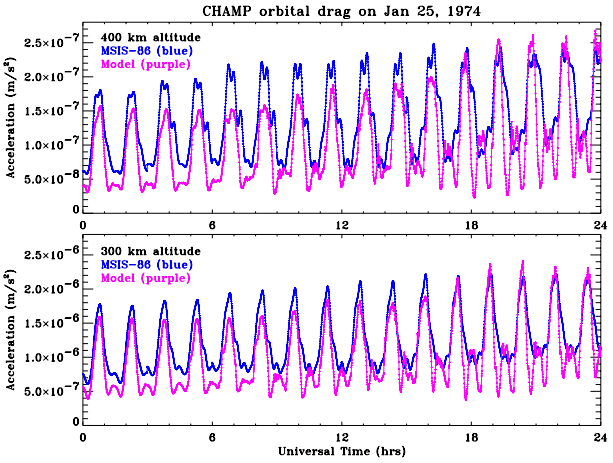

Figure 8: Acceleration estimates due to neutral air drag derived from the MSIS–86 model (blue) and from the GSM TIP model (purple) at 400 km (a) and 300 km altitude (b).

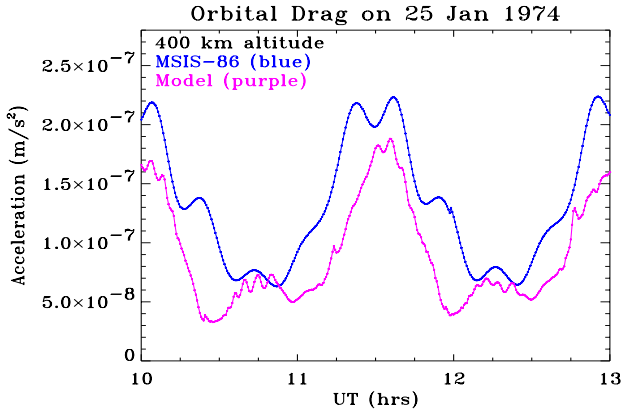

Figure 9: The Model curve (purple) shows details such as the gravity waves (around 10:45 UT) which will be resolvable even at this high altitude.

5. CONCLUSIONS

- The comparison between the MSIS–86 model and the GSM TIP model shows significant differences during disturbed times which lead to markedly different orbital decay predictions.
- The GSM TIP predicts detailed density structures (gravity waves) which propagate equatorward.
- The sensitivity of the accelerometer on board CHAMP is high enough ($< 1 \times 10^{-8} m/s^2$) to check the validity of thermospheric models and resolve the fine structure of density variations.
- The CHAMP instrumentation with its magnetometers and the ion drift–meter can provide the input parameters for the GSM TIP from in–situ measurements.

References

Förster, M., Fatkullin, M. N., Gasilov, N. A., & Schwarz, U. 1992. Medium–scale wave–like irregularities of electron density and electron temperature in the upper ionosphere at subauroral and high latitudes during different phases of the magnetic storm of January 1974. *Can. J. Phys.*, **70**, 582–594.

Hedin, A. E. 1987. MSIS-86 thermospheric model. *J. Geophys. Res.*, **92**, 4649–4662.

Namgaladze, A. A., Korenkov, Yu. N., Klimenko, V. V., Karpov, I. V., Bessarab, F. S., Surotkin, V. A., Glushchenko, T. A., & Naumova, N. M. 1988. Global model of the thermosphere–ionosphere–protonosphere system. *Pure Appl. Geophys.*, **127**, 219–254.

Namgaladze, A. A., Korenkov, Yu. N., Klimenko, V. V., Karpov, I. V., Surotkin, V. A., & Naumova, N. M. 1991. Numerical modelling of the thermosphere–ionosphere–protonosphere system. *J. Atmos. Terr. Phys.*, **53**, 1113–1124.

Wei, Deng, & Förster, M. 1989. Changes of thermospheric composition and the response of the ionosphere during the magnetic storm of January, 1974. *Gerlands Beitr. Geophysik*, **98**, 240–250.

Weimer, D. R., Maynard, N. C., Burke, W. J., & Liebrecht, C. 1990. Polar cap potentials and the auroral electrojet indices. *Planet. Space Sci.*, **38**, 1207–1222.